

The Effect of High Column Density Systems on the Measurement of the Lyman α Forest Correlation Function

Andreu Font-Ribera,^{a,b,c} Jordi Miralda-Escudé^{d,e}

^aInstitut de Ciències de l'Espai (IEEC-CSIC), E. de Ciències, Torre C5, Bellaterra, Catalonia, Spain.

^bInstitute of Theoretical Physics, University of Zürich, Winterthustrasse 190, Zurich, Switzerland

^cLawrence Berkeley National Laboratory, 1 Cyclotron Road, 94720 Berkeley, California, U.S.A.

^dInstitució Catalana de Recerca i Estudis Avançats, Catalonia

^eInstitut de Ciències del Cosmos (IEEC/UB), Barcelona, Catalonia

E-mail: font@ieec.uab.es

Abstract. We present a study of the effect of High Column Density (HCD) systems on the Ly α forest correlation function on large scales. We study the effect both numerically, by inserting HCD systems on mock spectra for a specific model, and analytically, in the context of two-point correlations and linear theory. We show that the presence of HCDs substantially contributes to the noise of the correlation function measurement, and systematically alters the measured redshift-space correlation function of the Ly α forest, increasing the value of the density bias factor and decreasing the redshift distortion parameter β_α of the Ly α forest. We provide simple formulae for corrections on these derived parameters, as a function of the mean effective optical depth and bias factor of the host halos of the HCDs, and discuss the conditions under which these expressions should be valid. In practice, precise corrections to the measured parameters of the Ly α forest correlation for the HCD effects are more complex than the simple analytical approximations we present, owing to non-linear effects of the damped wings of the HCD systems and the presence of three-point terms. However, we conclude that an accurate correction for these HCD effects can be obtained numerically and calibrated with observations of the HCD-Ly α cross-correlation. We also discuss an analogous formalism to treat and correct for the contaminating effect of metal lines overlapping the Ly α forest spectra.

Keywords: cosmology: large-scale structure — cosmology: spectroscopic surveys — galaxies: intergalactic medium — galaxies: absorption systems

Contents

1	Introduction	1
2	Model for the High Column Density systems	3
2.1	Ly α mock spectra	3
2.2	Column density distribution and Doppler parameters	4
2.3	Clustering of HCDs	6
3	Effect on the measured Lyα correlation function	7
3.1	Increase of measurement errors	8
3.2	Systematic effect on the measured bias parameters	9
4	Analytical description	11
4.1	Impact on the correlation function	12
4.2	Effective bias parameters	13
4.3	Relation to the bias of host halos	14
4.4	Corrections for the two-point linear terms	15
4.5	Application to the measurement on mock spectra	16
4.6	The non-linear effect of the damped wings	18
5	Effect of Metal Lines	19
6	Conclusions	20
A	Appendix: Clustering of the HCD systems	23
A.1	Biases of the Gaussian field	24
A.2	Biases of the peaks	25

1 Introduction

Observations of the correlation function of the Ly α forest in redshift space from multiple spectra is emerging as a powerful tool to explore the large-scale structure of the universe

at high redshift. This development has been led by the BOSS survey, part of the SDSS-III collaboration [1], which is obtaining optical spectra of 160,000 quasars at $z > 2.1$ for the principal purpose of studying the Ly α forest absorption and measuring its power spectrum. The redshift space power spectrum of the fluctuations in the fraction of transmitted flux, F , has a complex form on small scales that is affected by non-linear gravitational evolution, thermal broadening, the non-linear relation between F and the optical depth, and complex physical processes such as galactic winds. But on large scales, the power spectrum should be simply related to the mass power spectrum in the linear regime, P_L , through two biasing parameters [2]:

$$P_\alpha(k, \mu_k) = b_\alpha^2 (1 + \beta_\alpha \mu_k^2)^2 P_L(k) , \quad (1.1)$$

where k and μ_k are the modulus and angle cosine relative to the line of sight of the wave vector in redshift space, b_α is the bias factor relating the amplitude of fluctuations in F to the relative amplitude of density fluctuations, and β_α is the redshift distortion parameter. This form of the linear power spectrum in redshift space is the same as that for discrete tracers of the density field [3], except that β_α depends also on the bias parameter for the peculiar velocity gradient, b_η . Recently, the first measurement of b_α and β_α for the Ly α forest was reported by [4] from the first year of BOSS data, and more accurate measurements are expected in the near future.

The values of b_α and β_α as a function of redshift can be predicted in principle from numerical simulations of the Ly α forest [2, 5], and they depend on the detailed small-scale physical processes in the intergalactic medium. Comparison of the predicted values with the observed ones will therefore test these physical processes. However, in practice the observed absorption spectra are affected not only by the low-density gas producing the Ly α forest, but also by higher density systems that give rise to absorption lines of high column density, observed as Lyman limit systems (hereafter LLS, with column densities $N_{HI} > 10^{17.2} \text{ cm}^{-2}$) and damped Ly α systems (hereafter DLA, with $N_{HI} > 10^{20.3} \text{ cm}^{-2}$). These systems, as well as the lower column density Ly α forest, produce also metal absorption lines, some of which appear in the region of the Ly α absorption and add to the contamination of the measurement of the Ly α power spectrum.

The presence of high column density systems (hereafter referred to as HCDs, meaning both LLS and DLAs) has a similar effect on the Ly α power spectrum as the well-known “fingers of God” in galaxy redshift surveys: on small, non-linear scales, galaxies accumulate in high-density clusters with an internal velocity dispersion, appearing in redshift space as highly elongated structures along the line of sight. This induces contours of the correlation function that are also elongated along the line of sight on small scales, precisely the opposite to the squashing effect on the correlation function contours induced by the Kaiser linear term in the power spectrum that is prevalent on large scales. In the case of absorption spectra, the damped wings of the HCDs may similarly spread the correlation function along the line of sight. However, contrary to the “fingers of God” in galaxy surveys, the effects of damped wings extend out to all large scales in the Ly α forest, owing to their power-law absorption profiles. Metal lines can also cause an elongation of contours when they overlap the Ly α forest and introduce bumps in the correlation function near the line of sight around the separation that corresponds to the wavelength difference between the metal and the Ly α lines. In addition to this effect, there is also the purely linear fact that if the HCDs have a different redshift distortion factor than the Ly α forest, the correlation of the combined

transmission will display an averaged redshift distortion factor of the absorber populations that are contributing to the total absorption.

While most previous work studied the effect of HCDs on the power spectrum along the line-of-sight [6, 7], this paper focuses on the impact of HCDs on the linear bias factors of the Ly α forest. Their effect on the measured power spectrum is determined by the fact that HCDs are correlated with the underlying mass distribution and therefore with the Ly α forest intergalactic absorption. Their presence also adds additional noise to any power spectrum measurements. The impact of metal-line absorbers is also important and was briefly discussed in [4]. Here we present a description of the expected effect, and we describe a method to correct it in the Ly α correlation measurements.

In Section 2 we present a method to introduce HCD systems in Ly α mock spectra. The effect of HCD in the measurement of the Ly α forest correlation inferred from mocks is presented in Section 3. An analytical description of this effect is described in Section 4. Finally, the impact of metal lines is discussed in Section 5.

A standard flat Λ CDM cosmology is used in this paper with the following parameters: $h = 0.72$, $\Omega_m = 0.281$, $\sigma_8 = 0.85$, $n_s = 0.963$, $\Omega_b = 0.0462$.

2 Model for the High Column Density systems

The impact of HCDs on the correlation function of Ly α absorption depends on their column density and Doppler parameter distribution, and on the way they are distributed in space relative to the underlying Ly α forest. In this section, we describe the method we use to introduce these systems in mock Ly α absorption spectra. We first briefly summarize the method to generate the Ly α forest mock spectra [8]. Then we describe our model distributions for HCDs, and the way they are inserted in the mock spectra with a correlation with the Ly α absorption field.

2.1 Ly α mock spectra

The reader is referred to [8] for a full account of the method we use to generate mock Ly α spectra with any specified three-dimensional flux power spectrum and flux probability distribution function. Here we highlight the features that are most important for this paper. The method consists of two steps:

- A Gaussian random field $\delta_g(x)$ is generated for the set of specified lines of sight.
- The field is transformed to a new variable $F(\delta_g)$ constrained to the range $0 < F < 1$, determined by the condition of matching the model probability distribution of F . The power spectrum for the Gaussian variable δ_g is chosen so that the final flux power spectrum of F is the desired one.

In general, as described in [8], a third step can be applied where one interpolates the value of F between lines of sight generated at different redshifts to simulate the effect of redshift evolution and the fact that the lines of sight are not parallel. This third step is not

included in this paper. The lines of sight are generated as parallel lines at a fixed redshift of $z = 2.3$, with a value of the mean transmission fixed at $F_\alpha = 0.791$, in order to study the effect of the HCD systems without introducing additional complexities into the mocks.

We use here the same flux power spectrum $P_\alpha(k, \mu_k)$ from [2],

$$P_\alpha(k, \mu_k) = b_\alpha^2 (1 + \beta_\alpha \mu_k^2)^2 P_L(k) D(k, \mu_k), \quad (2.1)$$

where $P_L(k)$ is the linear matter power spectrum, μ_k is the cosine of the angle of the Fourier vector from the line of sight, and $D(k, \mu_k)$ is a small scale non-linear term that was fitted to the results of numerical simulations in [2]. We use the central values for the model parameters from the first row of Table 1 in [2], after applying a small correction to the bias parameter for the difference in redshift (the biases in [2] are computed at $z = 2.25$) by assuming that the power spectrum amplitude evolves as $(1+z)^{3.8}$ [4], which implies, neglecting the influence of the cosmological constant on the growth factor at this redshift, that the bias b_α evolves as $(1+z)^{2.9}$. The resulting bias parameters are $b_\alpha = -0.1375$ and $\beta_\alpha = 1.58$.

2.2 Column density distribution and Doppler parameters

A large part of the contamination by HCD systems on the Ly α forest correlation arises from the damped wings, which depend exclusively on the column density. It is therefore most important to use a model that reproduces the observed column density distribution of these systems. The large number of quasars observed in the Sloan Digital Sky Survey has in recent years allowed good determinations of this distribution [9, 10].

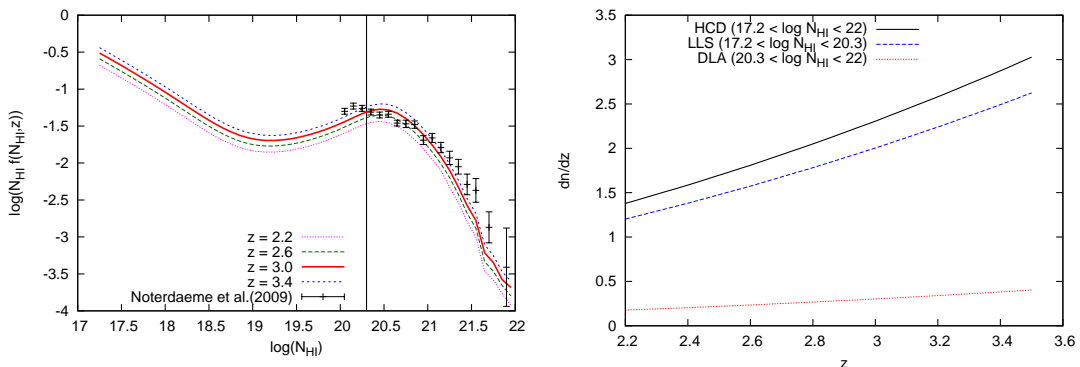


Figure 1. *Left:* Number of HCD systems per unit of column density N_{HI} and unit of "absorption distance" as defined in the text. The lines show the values for our model, at $z = 2.2$, $z = 2.6$, $z = 3$ and $z = 3.4$. The vertical line indicates the standard separation between DLA and LLS. Points with errorbars show the observational determination in [10], with a central redshift of $z \approx 3$. *Right:* Number of systems per unit of redshift in the indicated column density ranges as a function of redshift.

Here we use the neutral hydrogen column density distribution used in [6], which is based on an analytical expression derived in [11] that assumes an intrinsic power-law distribution of the total hydrogen column density and takes into account the self-shielding effects on the neutral column density, and is calibrated to match the observations of DLAs in [9]. In figure 1, the column density distribution in this model is shown at different redshifts (*left panel*),

together with the observations of [10]. In this figure we plot the frequency distribution per unit of column density and "absorption distance" X , defined as

$$dX \equiv \frac{H_0}{H(z)}(1+z)^2 dz, \quad (2.2)$$

since this is the function presented in the SDSS analysis. Self-shielding causes the flattening of the distribution in the column density range of 10^{18} to 10^{20} cm^{-2} . In the right panel we plot the number of systems as a function of redshift integrated over various column density ranges.

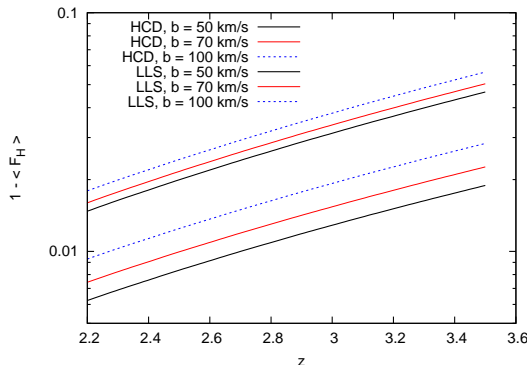


Figure 2. Mean absorption caused by HCD systems for several values of b_D . Lower lines include systems with $N_{HI} < 10^{20.3} \text{ cm}^{-2}$ only; upper lines include all systems.

As discussed in section 4, the perturbation caused by HCD systems on the Ly α correlation increases with their contribution to the mean effective optical depth, $\bar{\tau}_{eH} = -\log(\bar{F}_H)$, which depends on the velocity dispersions in addition to the column densities of the systems. Here we calculate its value as a function of redshift for different values of the Doppler parameter b_D , and the column density distribution used in this study. Defining $W(N_{HI}, b_D)$ as the rest-frame equivalent width according to the standard curve of growth of an absorber with a Gaussian distribution of velocities, the mean absorbed fraction by HCDs (assuming their positions are uncorrelated) is

$$\bar{\tau}_{eH}(z) = \int dN_{HI} \frac{d^2 n(z, N_{HI})}{dN_{HI} dz} \frac{W(N_{HI}, b_D)}{\lambda_\alpha} (1+z). \quad (2.3)$$

This effective optical depth is plotted in Figure 2 as a function of redshift, separately for all the systems (HCD) and including only systems with $N_{HI} < 10^{20.3} \text{ cm}^{-2}$ (designated here as LLS), for three different values of b_D . The contribution from systems that are not included in the definition of DLAs to $\bar{\tau}_{eH}$ is about half of the total, and increases with b_D . At the redshift of our mocks, the total effective optical depth from HCDs is close to 2%.

In the mocks of this paper we use a value of $b_D = 70 \text{ km s}^{-1}$, a representative value for DLAs (see [12]). We note that the value of b_D actually has a large dispersion and its mean depends on the column density (being smaller for lower column density systems). We shall not examine the possible dependence of the effects on the correlation function we study on the distribution of b_D , but we note that most of these effects arise from the damped wings, which are unaffected by the velocity dispersion. Better observational constraints on $\bar{\tau}_{eH}$ in the future will help quantify the effect of HCDs more accurately.

2.3 Clustering of HCDs

While the effect of HCDs on increasing the noise in the measurement of the Ly α correlation can be adequately estimated by simply placing the absorption systems randomly in the mock spectra, the systematic effect on the correlation is induced only by their clustering. On large scales, this systematic effect on the total measured correlation should be governed by the bias factors of the HCDs.

Here we use a simple method to insert these systems in the mock spectra, by placing them only in a fraction ν of pixels where the optical depth is above a certain threshold, $\tau > \tau_c$. For a fixed distribution function of $F = \exp(-\tau)$, the value of ν determines the critical optical depth τ_c or, equivalently, a critical transmitted flux fraction F_c :

$$\nu = \int_{\tau_c}^{\infty} d\tau p_{\tau}(\tau) = \int_0^{F_c} dF p_F(F) \quad (2.4)$$

The dependence of the probability distribution function p_{τ} on redshift implies that the threshold τ_c for hosting a HCD depends also on redshift. In this paper we do not include redshift evolution to avoid complications, and we analyze the effect of HCDs at the single redshift $z = 2.3$, although our method generally incorporates redshift evolution when detailed mocks of the BOSS data are required. Here we generally use $\nu = 0.01$ (which yields $\tau_c \approx 12$ at $z = 2.3$), except for one model where we increase the HCD bias by changing to $\nu = 0.002$.

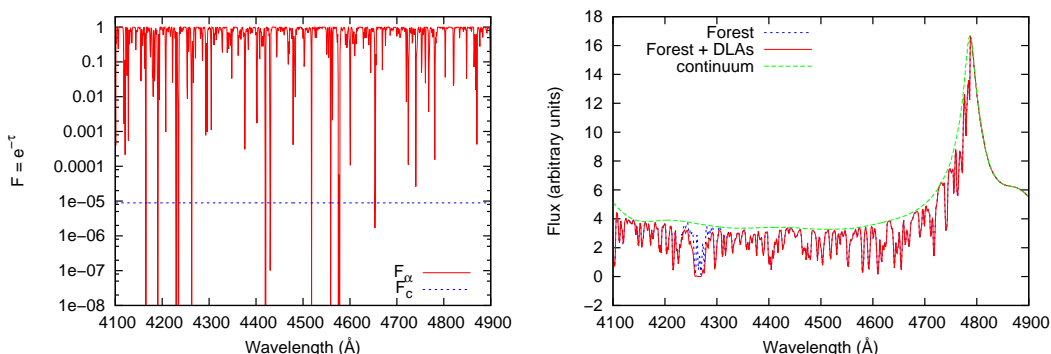


Figure 3. Left: Example of mock Ly α absorption field F (red) and the threshold F_c to host a HCD for $\nu = 0.01$ (dotted blue). Right: Mock spectrum for the same line of sight. The green line is the quasar continuum, and the blue line is the absorption due to Ly α forest, smoothed with the spectrograph resolution as described in ([8]). The red line includes absorption by a HCD.

The HCD are randomly inserted in the mock spectra in pixels with $\tau > \tau_c$, assigning column densities to them that follow the distribution shown in Figure 1. A typical mock spectrum is shown in Figure 3. The left panel shows the spectrum of F due to the Ly α forest and value of F_c . Systems can only be located in a few narrow spikes in optical depth covering a fraction ν of the spectrum. The right panel shows the spectrum in linear units after multiplying by the quasar continuum and smoothing with the resolution of the BOSS spectrograph, as described in [8]. A HCD has been randomly assigned to one of the peaks that cross the threshold in the first figure (in this case, the peak at $\lambda \sim 4260$ Å), and has been included in the total absorption.

As shown in Appendix A, the large-scale clustering of the HCDs inserted in this way in the mock spectra follows linear theory with a bias factor b_h that depends on ν and on the probability distribution function of F (which is modelled as a lognormal function in our mocks, as described in [8]), and with a redshift distortion parameter equal to that of the Ly α forest, $\beta_h = \beta_\alpha$. We note that this is a consequence of the simple procedure we use for inserting the HCDs, and that in reality their bias factor and redshift distortion parameter should depend on the distribution of their host halos and the selection effects involved in their detection. For our fiducial value of $\nu = 0.01$, the bias of the HCDs inserted in our mocks is $b_h = 1.21$, while for a more extreme value of $\nu = 0.002$ the bias is $b_h = 1.43$.

3 Effect on the measured Ly α correlation function

We now investigate the impact of HCDs on the Ly α correlation function, by measuring it directly in mock spectra. We generate 100 realizations of a mock survey with an area of 200 deg^2 . Quasars are distributed following the luminosity function from [13], with a total quasar density of 22 deg^{-2} , over the redshift range $2.15 < z < 3.5$. We use the same definition of the Ly α forest as [4], i.e., the rest-frame wavelength range $1041 \text{ \AA} - 1185 \text{ \AA}$. We also apply a cut at an observed wavelength of 3600 \AA , close to the end of the BOSS spectrograph.

As previously mentioned, the Ly α absorption mock spectra are generated with no redshift evolution and assuming that the lines of sight are parallel. HCD systems are inserted with the method explained above, and we measure the correlation function in 150 linear bins in r of width $1 h^{-1} \text{ Mpc}$, and 20 linear bins in $\mu = \cos \theta$. The correlation function in each bin A is estimated by averaging over all pixel pairs with a separation that is within the bin A ,

$$\hat{\xi}_A = \frac{\sum_{i,j \in A} \delta_{Fi} \delta_{Fj}}{\sum_{i,j \in A} 1}, \quad (3.1)$$

where the indices i or j label all pixels in the Ly α forest region. Here the weights are all set equal to unity because the mock spectra are noiseless.

In Figure 4 we show the mean measurement of the correlation function in the $N = 100$ realizations, before and after adding the HCD systems, after averaging the original bins into wider ones with $\Delta r = 5 h^{-1} \text{ Mpc}$ and $\Delta \mu = 0.2$. The errorbars are computed for the mean, equal to the dispersion among realizations divided by $\sqrt{N - 1}$.

There are two main effects caused by the HCD systems on the measured correlation function: the measurement error is increased, and the correlation function is systematically altered from the true value of the Ly α forest alone. We first quantify the increase in the statistical error in §3.1, and then we study the systematic effects on the two Ly α bias parameters in §3.2. We shall not examine in this paper the systematic effect on the inferred shape of the linear power spectrum in equation (2.1). However, as seen in Figure 4, the systematic change in the correlation function is not limited to the values of the bias parameters but can affect the broadband shape in a generic way, even at very large scales because of the extended damped wings of HCDs. Therefore, any other constraints that are obtained from measurements of the Ly α forest power spectrum are in general subject to a correction for the impact of HCDs.

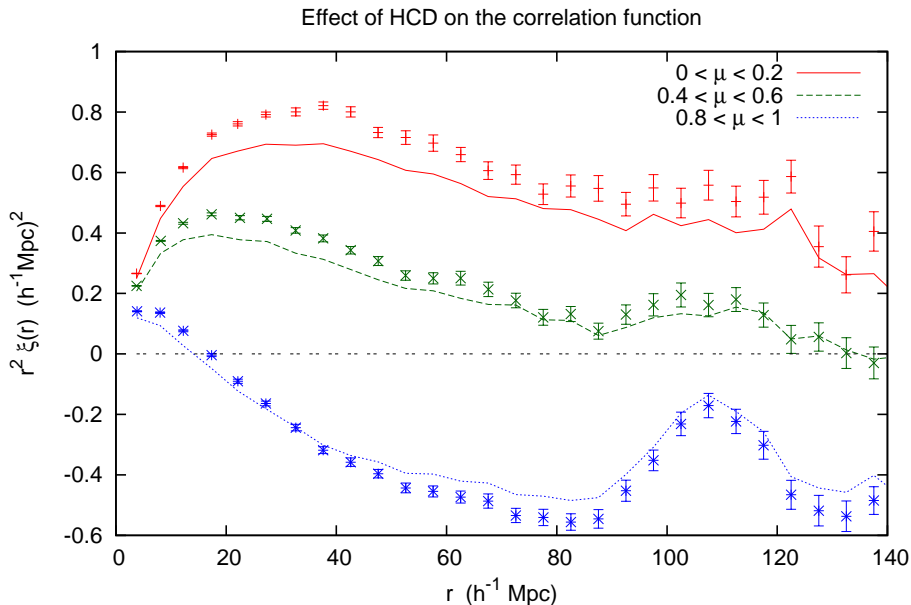


Figure 4. Correlation function measured from mock spectra with inserted high column density systems, shown in 3 angular bins, with errorbars indicating the error for the mean of 100 mocks with 200 square degrees each. Thin lines show the mean measured in the same mock spectra without the HCD systems.

3.1 Increase of measurement errors

In Figure 5, the increase in the error of the measured correlation function due to HCD systems is shown. The error is for the mean of all the $N = 100$ realizations.

The increase of the errorbars in the absence of observational noise is $\sim 30 - 50\%$. Because errors are added quadratically, this means that the contribution from HCD to the total noise is comparable to that arising from the intrinsic small-scale variance of the Ly α forest. In an actual survey like BOSS, the error budget of the correlation function includes also observational noise. For instance, it was shown in [8] that a level of noise comparable to that in the BOSS survey increases the errorbars by $\sim 30\%$. In this case, the total error budget has three comparable contributions from the intrinsic Ly α forest variance, HCD systems and observational noise.

We have performed some tests on the origin of the additional errors introduced by HCDs in the correlation measurement. If DLAs (with $N_{HI} > 10^{20.3} \text{ cm}^{-2}$) are eliminated from the HCDs that are inserted (a model we designate as NO DLA, see Table 1 below), then the increase of errors is reduced to 15%. If the damped wings of all the HCDs are eliminated (keeping only their saturated Gaussian profiles, a model we designate as NO WINGS), then the error increase is further reduced to 5 to 10% of the total. This shows that the damped wings are the dominant reason for increased errors in the correlation measurements.

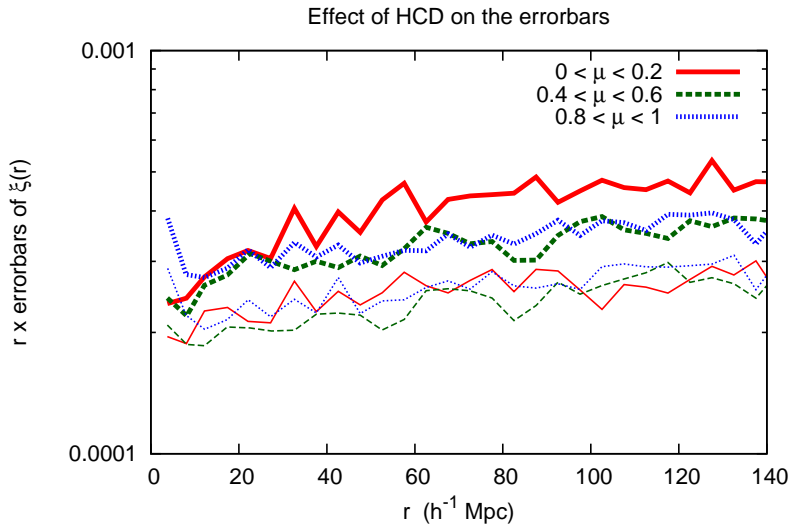


Figure 5. Errors in the correlation function measured from mock spectra with (thick lines) and without (thin lines) high column density systems, in 3 angular bins. The errors have been multiplied by r .

3.2 Systematic effect on the measured bias parameters

We now discuss the result of fitting the correlation function in the mocks with inserted HCD systems with the equation for the linear theory power spectrum,

$$P_F(k, \mu_k) = b_F^2 (1 + \beta_F \mu_k^2)^2 P_L(k) , \quad (3.2)$$

where now b_F and β_F are the bias parameters for the total absorption field, including Ly α forest and HCD absorption.

The precise procedure for fitting the correlation function by χ^2 minimization carried out in [4] requires a complex and expensive calculation of the covariance matrix of the correlation values measured in each pair of bins. Here we use a simplified procedure, where only the diagonal elements of the covariance matrix of the binned correlation function are taken into account to minimize χ^2 . This allows us to quickly examine a large number of realizations of many different models. However, in order to obtain the errors in the fitted bias parameters, we rely on bootstrap combinations of the 100 realizations of the survey. In other words, we simply use the dispersion in the fitted values of the parameters that are obtained in different realizations. Using the full covariance matrix should lead to reduced errors of the fitted parameters, but we find that this error reduction is not large and that the systematic impact of HCDs is adequately reflected in the results of the fits that use the diagonal elements of the covariance matrix only.

The results of the fits for the bias parameters are listed in Table 1 for a variety of models with different properties of the HCDs. The mean effective optical depth and the bias of the selected pixels for inserting HCDs are listed initially in Table 1. The additional variable C given in the Table is the correlation of the Ly α and HCD transmission fluctuation at zero

separation [see eq. (4.2) in the next section, where this will be used; we note here that the mean transmitted fraction \bar{F} is slightly reduced by the insertion of HCDs according to eq. (4.3), where $F_H = \exp(-\bar{\tau}_{eH})$]. As shown in [4], the combination of parameters that is most accurately determined from the 3D correlation function is $b_F(1 + \beta_F)$. We therefore list the average best fit values of b_F , β_F and $b_F(1 + \beta_F)$, each one with the error directly obtained from the bootstrap analysis. We note that the linear function used to fit the correlation function in equation (3.2) neglects the non-linear term $D(k, \mu_k)$ that is present in the power spectrum used to generate the mocks (eq. 2.1). We therefore do not expect to recover exactly the input values of the bias factors even when no HCDs are included. To minimize the non-linear effects, our fit to the correlation function uses only bins at $r > 10$ Mpc/h.

Model	$\bar{\tau}_{eH}$	b_h	C	b_F	β_F	$b_F(1 + \beta_F)$
NO HCD	0	–	–	-0.1472 ± 0.0005	1.550 ± 0.009	-0.3756 ± 0.0003
FIDUCIAL	0.017	1.21	0.0034	-0.1678 ± 0.0013	1.374 ± 0.018	-0.3984 ± 0.0008
HIGH BIAS	0.016	1.43	0.0032	-0.1732 ± 0.0009	1.306 ± 0.011	-0.3994 ± 0.0009
NO DLA	0.009	1.21	0.0029	-0.1563 ± 0.0006	1.495 ± 0.011	-0.3902 ± 0.0004
NO WINGS	0.007	1.21	0.0033	-0.1519 ± 0.0006	1.546 ± 0.010	-0.3867 ± 0.0005

Table 1. Fitted bias parameters for mocks with different models for the inserted HCDs. The variable C is defined in the next section.

The first model in Table 1 (labeled NO HCD) does not include any HCD systems. The recovered values of the bias parameters are very close to the input ones, $b = -0.1375$ and $\beta = 1.58$. The small differences are due to the non-linear term. The second row is for our fiducial model, where HCDs are added following the column density distribution described in the previous section in regions of high optical depth with a spectral filling factor $\nu = 0.01$, corresponding to a bias factor $b_h = 1.21$. The HCDs in the fiducial model induce an increase of the bias parameter b_F of 14%, and a reduction of the redshift distortion parameter β_F of 11%.

The third model, labeled HIGH BIAS, forces the HCDs into a smaller fraction of the Ly α forest spectra, $\nu = 0.002$, increasing their bias factor to $b_h = 1.43$. The value of b_F now increases by 18% and β_F decreases by 16%. The systematic impact of HCDs is therefore increased as their bias factor increases. We remind that here we have to keep the value of β_h for the HCDs equal to that of the Ly α forest, because of the way they are inserted in the mock spectra. In reality β_h should be close to $1/b_h$ and, as we shall see below this should further enhance the impact of the HCDs on the value of β_H .

The fourth row gives the result for a model where only systems with a column density $N_{HI} < 10^{20.3} \text{ cm}^{-2}$ are included (labeled NO DLA), using again $\nu = 0.01$. In other words, the systems generally referred to as damped Ly α systems are not included. The lower column density systems producing the remaining effect, even though they are not generally identified as DLAs, obviously produce weak damped absorption wings as well. These weak systems are responsible for an increase of the bias factor of 6% and a decrease of β_F of 3.5%, i.e., ~ 30 to 40% of the total effect of all the systems in the FIDUCIAL model. In a survey with spectra with the resolution and signal-to-noise of BOSS, most of the systems with $N_{HI} > 10^{20.3} \text{ cm}^{-2}$ can be individually identified and removed from the sample in order to test for their impact on the correlation function, but most of the systems with lower column densities cannot

be reliably identified. Therefore, removing the identified DLAs from the sample will not completely eliminate the systematic errors in the Ly α correlation induced by HCDs. We note here that if one chooses to eliminate all the spectra containing DLAs in a Ly α forest survey like BOSS, then the measured correlation is also systematically biased in a different way because the Ly α forest is correlated with the presence of HCDs.

The final model (fifth row, labeled NO WINGS) inserts all the HCDs only with their Gaussian profiles (with the fixed Doppler parameter $b_D = 70 \text{ km s}^{-1}$), with no damped wings. In this case the impact on the recovered bias parameters is smaller, especially for β_F which is practically not affected. This shows that the main impact of HCDs on the correlation function is through the damped wings of the absorbers.

4 Analytical description

We now present an analytical formulation to evaluate the effect of the high column density systems (HCDs) on the correlation function of the flux transmission fraction, F . Even when the analytical results require making certain approximations, they are highly useful to provide an interpretation of the numerical results and an understanding of the dependence to be expected with any variations of the model for the column density distribution and bias parameters of the HCDs.

We start by introducing some useful notation. The transmitted fraction at a point \mathbf{x} in a spectrum is $F(\mathbf{x}) = \bar{F} [1 + \delta_F(\mathbf{x})]$, where \bar{F} is the mean value of F at a certain redshift. We divide this total transmission into a contribution F_H from HCDs, defined as absorption systems with a column density $N_{HI} > 1.6 \times 10^{17} \text{ cm}^{-2}$ (i.e., a continuum optical depth greater than unity at the Lyman limit), and a contribution F_α from the Ly α forest, defined as all the remaining Ly α absorption by atomic hydrogen. Hence, $F(\mathbf{x}) = F_H(\mathbf{x}) F_\alpha(\mathbf{x})$. We ignore here the presence of metal lines; these will be considered briefly in §5. We note that the precise column density at which this conventional separation between Ly α forest and HCDs is made does not affect our results. The important point is that the Ly α forest absorption is dominated by systems with much lower column density than the Lyman limit threshold, and the HCDs absorption is dominated by systems with much higher column density than this threshold. Therefore, the precise choice for the threshold is not crucial.

Let the transmitted fraction of the Ly α forest be $F_\alpha(\mathbf{x}) = \bar{F}_\alpha [1 + \delta_\alpha(\mathbf{x})]$, and the transmitted fraction of the HCDs be $F_H(\mathbf{x}) = \bar{F}_H [1 + \delta_H(\mathbf{x})]$. We then have,

$$F(\mathbf{x}) = \bar{F} [(1 + \delta_F(\mathbf{x})) = F_\alpha(\mathbf{x}) F_H(\mathbf{x}) = \bar{F}_\alpha [1 + \delta_\alpha(\mathbf{x})] \bar{F}_H [1 + \delta_H(\mathbf{x})] . \quad (4.1)$$

Being tracers of the same underlying density field, the fields δ_α and δ_H are correlated,

$$C \equiv \langle \delta_\alpha(\mathbf{x}) \delta_H(\mathbf{x}) \rangle \neq 0 , \quad (4.2)$$

and the relation between \bar{F} and \bar{F}_α is

$$\bar{F} = \langle F \rangle = \bar{F}_\alpha \bar{F}_H (1 + C) . \quad (4.3)$$

Hence, the variable $\delta_F(\mathbf{x})$ can be expressed as

$$1 + \delta_F(\mathbf{x}) = \frac{F(\mathbf{x})}{\bar{F}} = \frac{[1 + \delta_\alpha(\mathbf{x})] [1 + \delta_H(\mathbf{x})]}{1 + C} . \quad (4.4)$$

4.1 Impact on the correlation function

We can now write an expression for the correlation function of δ_F at two points \mathbf{x}_1 and \mathbf{x}_2 as a function of the separation $\mathbf{r}_{12} = \mathbf{x}_1 - \mathbf{x}_2$:

$$\begin{aligned}
1 + \xi_F(\mathbf{r}_{12}) &= \langle [1 + \delta_F(\mathbf{x}_1)] [1 + \delta_F(\mathbf{x}_2)] \rangle \\
&= (1 + C)^{-2} \langle [1 + \delta_\alpha(\mathbf{x}_1)] [1 + \delta_H(\mathbf{x}_1)] [(1 + \delta_\alpha(\mathbf{x}_2))] [(1 + \delta_H(\mathbf{x}_2))] \rangle \\
&= (1 + C)^{-2} [1 + 2C + \xi_\alpha(\mathbf{r}_{12}) + 2\xi_{\alpha H}(\mathbf{r}_{12}) + \xi_H(\mathbf{r}_{12}) \\
&\quad + 2\xi_{3\alpha}(\mathbf{r}_{12}) + 2\xi_{3H}(\mathbf{r}_{12}) + \xi_4(\mathbf{r}_{12})] ,
\end{aligned} \tag{4.5}$$

where we have defined:

$$\begin{aligned}
\xi_\alpha(\mathbf{r}_{12}) &= \langle \delta_\alpha(\mathbf{x}_1) \delta_\alpha(\mathbf{x}_2) \rangle , \\
\xi_{\alpha H}(\mathbf{r}_{12}) &= \langle \delta_\alpha(\mathbf{x}_1) \delta_H(\mathbf{x}_2) \rangle , \\
\xi_H(\mathbf{r}_{12}) &= \langle \delta_H(\mathbf{x}_1) \delta_H(\mathbf{x}_2) \rangle , \\
\xi_{3\alpha}(\mathbf{r}_{12}) &= \langle \delta_\alpha(\mathbf{x}_1) \delta_H(\mathbf{x}_1) \delta_\alpha(\mathbf{x}_2) \rangle , \\
\xi_{3H}(\mathbf{r}_{12}) &= \langle \delta_\alpha(\mathbf{x}_1) \delta_H(\mathbf{x}_1) \delta_H(\mathbf{x}_2) \rangle , \\
\xi_4(\mathbf{r}_{12}) &= \langle \delta_\alpha(\mathbf{x}_1) \delta_H(\mathbf{x}_1) \delta_\alpha(\mathbf{x}_2) \delta_H(\mathbf{x}_2) \rangle .
\end{aligned} \tag{4.6}$$

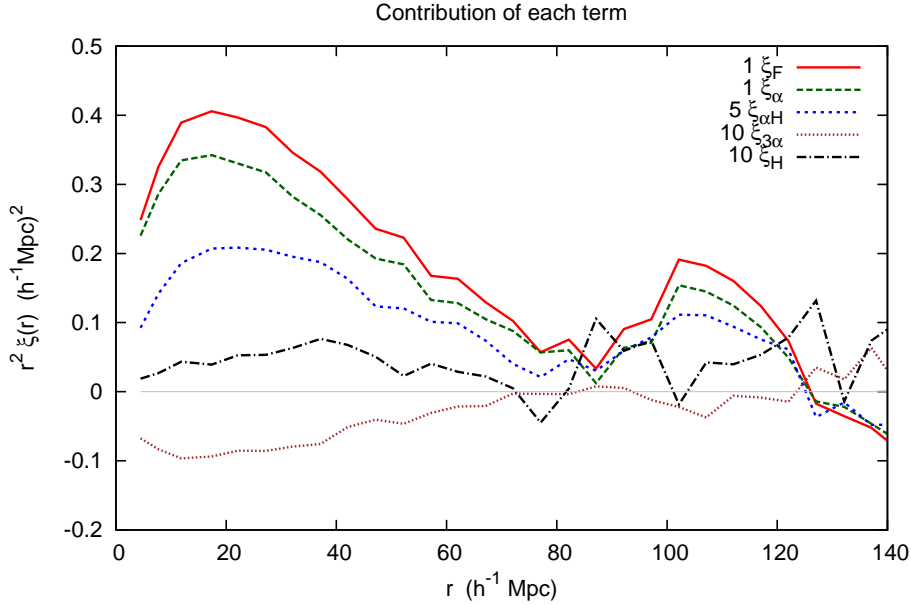


Figure 6. The total correlation function ξ_F and the contribution of the four largest terms in equation (4.6) in the numerical mock spectra.

We can compute the contribution of each of the 6 terms in equation 4.5 for the case of the mock spectra discussed in Sections 2 and 3. Figure 6 shows these contributions for our FIDUCIAL model, for the largest four terms only. The remaining two terms are substantially smaller and are omitted, and some of the terms are shown multiplied by a factor of 5 or 10 for better visualization. As seen in this figure, the leading correction due to the presence of HCDs is the term $\xi_{\alpha H}$, although the next largest term, $\xi_{3\alpha}$, is not much smaller.

4.2 Effective bias parameters

The full expression for the overall transmitted fraction correlation in equation (4.5) is highly complex, depending on a combination of 2, 3 and 4-point functions of the fields. While the 3-point and 4-point functions defined in equation (4.6) are difficult to characterize, the two-point correlation terms can be calculated in the limit of large scales assuming that linear theory applies. Then, each Fourier mode is multiplied by the factor $1 + \beta_i \mu_k^2$, with β_i being the redshift distortion factor of any tracer i [3]. With this in mind, we first aim to solve analytically the case when the 3-point and 4-point functions are negligible. Note, however, that in the case of our FIDUCIAL model in the numerical mocks, the 3-point term $\xi_{3\alpha}$ is actually larger than ξ_H and is smaller than $\xi_{\alpha H}$ by a factor of only ~ 5 , as shown in Figure 6. Furthermore, assuming linear theory is not actually accurate in this case, because the damped wings of the absorbers extend the correlation in the radial direction up to scales that can be arbitrarily large depending on the shape of the correlation function. The results obtained by considering only the linear 2-point terms should therefore be considered as no more than an initial guide, to be revised by the effects of the other terms (in particular $\xi_{3\alpha}$ for the observationally more relevant cases) and the validity of the linear approximation.

We therefore separate equation 4.5 as

$$\xi_F(\mathbf{r}_{12}) = \xi_2(\mathbf{r}_{12}) + \xi_{34}(\mathbf{r}_{12}) , \quad (4.7)$$

where the 2-point contribution is

$$\xi_2(\mathbf{r}_{12}) \equiv \frac{\xi_\alpha(\mathbf{r}_{12}) + 2\xi_{\alpha H}(\mathbf{r}_{12}) + \xi_H(\mathbf{r}_{12})}{(1+C)^2} , \quad (4.8)$$

and all the remaining 3-point and 4-point terms are included in ξ_{34} ,

$$\xi_{34}(\mathbf{r}_{12}) \equiv \frac{2\xi_{3\alpha}(\mathbf{r}_{12}) + 2\xi_{3H}(\mathbf{r}_{12}) + \xi_4(\mathbf{r}_{12}) - C^2}{(1+C)^2} . \quad (4.9)$$

Note that in the limit of large separation, ξ_4 approaches C^2 and therefore ξ_{34} vanishes.

Now, the Fourier transforms of the 2-point correlations ξ_α , ξ_H and $\xi_{\alpha H}$ yield their corresponding power spectra, which can be expressed in terms of the bias factors for each field. As described in [14] and [2], the general bias parameters of an absorption field arise by considering the first order expansion of the average of the mean transmission in a large scale, linear region that is conditioned to have density and peculiar velocity gradient perturbations δ and η . Therefore, in analogy to the Ly α forest, the bias factors for the HCD absorption field δ_H are

$$b_H = \frac{1}{\bar{F}_H} \frac{\partial F_H}{\partial \delta} , \quad b_{\eta H} = \frac{1}{\bar{F}_H} \frac{\partial F_H}{\partial \eta} , \quad (4.10)$$

and the redshift distortion parameter is

$$\beta_H = \frac{b_{\eta H} f(\Omega)}{b_H} , \quad (4.11)$$

where $f(\Omega)$ is the logarithmic derivative of the growth factor (see [3]). In linear theory, each Fourier mode of any tracer field is multiplied by the factor $b_i(1 + \beta_i \mu_k^2)$ relative to the mass field, and therefore the power spectra are

$$P_\alpha(k, \mu_k) = b_\alpha^2 (1 + \beta_\alpha \mu_k^2)^2 P_L(k) , \quad (4.12)$$

$$P_H(k, \mu_k) = b_H^2(1 + \beta_H \mu_k^2)^2 P_L(k) , \quad (4.13)$$

$$P_{\alpha H}(k, \mu_k) = b_\alpha b_H (1 + \beta_\alpha \mu_k^2)(1 + \beta_H \mu_k^2) P_L(k) . \quad (4.14)$$

Finally, the power spectrum P_2 of the 2-point terms is

$$\begin{aligned} \frac{P_2(k, \mu_k)}{P_L(k)} &= \frac{b_\alpha^2(1 + \beta_\alpha \mu_k^2)^2 + 2b_\alpha b_H(1 + \beta_\alpha \mu_k^2)(1 + \beta_H \mu_k^2) + b_H^2(1 + \beta_H \mu_k^2)^2}{(1 + C)^2} \\ &= b_2^2(1 + \beta_2 \mu_k^2)^2 , \end{aligned} \quad (4.15)$$

where we have defined

$$b_2 \equiv \frac{b_\alpha + b_H}{1 + C} , \quad (4.16)$$

and

$$b_2 \beta_2 \equiv \frac{b_\alpha \beta_\alpha + b_H \beta_H}{1 + C} . \quad (4.17)$$

In the absence of the term ξ_{34} and for linear theory, the relation between the bias factors measured from the observed correlation and that of the unpolluted Ly α forest is therefore remarkably simple. In principle, both b_H and β_H can be measured from the observable cross-correlation of the HCDs with the Ly α forest, and then the systematic effect of the HCDs on the total correlation can be corrected to obtain the Ly α forest bias parameters.

4.3 Relation to the bias of host halos

Whereas most of the Ly α forest absorption at $z > 2$ is associated with density fluctuations in the intergalactic medium forming an interconnected structure, the high column density systems should correspond to discrete, clearly identifiable overdense regions that have gravitationally collapsed, or halos. The natural question that arises is the relation of the bias factors defined in equation (4.10) to the host halo bias. We now address this question in order to predict the bias factors and the impact of the HCDs on the total power spectrum from equation (4.15).

We define new bias factors for the HCDs, which can be defined in an equivalent way for any other population of absorbers,

$$b'_H = \frac{1}{\bar{\tau}_{eH}} \frac{\partial \tau_{eH}}{\partial \delta} = -\frac{b_H}{\bar{\tau}_{eH}} ; \quad b'_{\eta H} = -\frac{b_{\eta H}}{\bar{\tau}_{eH}} , \quad (4.18)$$

where $\tau_{eH} = -\log F_H$ is the *effective* optical depth averaged over a large scale region with mean values of the density and peculiar velocity gradient perturbations δ and η , and $\bar{\tau}_{eH}$ is its average over all the universe, for $\delta = \eta = 0$. The effective optical depth is obtained by averaging F_H first, and then taking the logarithm. The bias is defined analogously to equation (4.10), but using the effective optical depth instead. These new bias factors for an absorption field can be interpreted in the usual way that bias factors for a collection of objects are interpreted: if the mean density perturbation increases by a fractional amount δ , while η is kept fixed, the mean effective optical depth of HCD absorption increases by a fractional amount $b'_H \delta$.

If the bias factor of the HCD host halos is b_h , this means that their number density should fluctuate on large scales as $\delta_h = b_h \delta$. If we now assume that the probability of observing an HCD when a halo of fixed mass is intercepted is independent of its large-scale environment (i.e., independent of δ and η), then the perturbation in the effective optical depth contributed by HCDs should be the same as that in the halo number density. In other words, we should have $b'_H = b_h$, and $b'_{\eta H} = 1$ in redshift space. More generally, this assumption holds only if the following two conditions are met:

1. The probability that the absorption profile of any HCD appears substantially blended with another one in the absorption spectrum is small. Here, substantially blended means that their profiles overlap in a region where their absorption optical depth is not much smaller than unity. This condition should in general be correct if $\bar{\tau}_{eH} \ll 1$ and the clustering of HCDs is not very strong.
2. The probability distribution of the column density in a halo of a fixed mass M_h is independent of its large-scale environment and is isotropic (i.e., it is independent of δ and η). In other words, the gas radial profile does not depend on the environment for fixed M_h , and the axes of any non-spherical gas distribution in the halos are not correlated with the principal axes of the deformation tensor of the surrounding large-scale structure. This assumption is likely to be not exactly true, because galaxy disks are known to be statistically aligned with the axes of their large-scale environment, which can affect their redshift distortion anisotropy [15], but the effect is probably very small.

Under these conditions, the transmission fluctuations due to HCDs should obey $\delta_H(\mathbf{x}) = -\bar{\tau}_{eH} \delta_h(\mathbf{x})$, and the bias factors are related by

$$b_H = -\bar{\tau}_{eH} b'_H = -\bar{\tau}_{eH} b_h ; \quad \beta_H = \frac{b_{\eta H} f(\Omega)}{b_H} = \frac{f(\Omega)}{b_h} . \quad (4.19)$$

In the rest of this Section, we assume that these relations hold, which is reasonable for HCDs in view of the conditions that are required, and that $\bar{\tau}_{eH} \ll 1$. Note that these new bias factors can be defined for the Ly α forest in the same way, and that they also provide a measure of the relative fluctuations in the Ly α effective optical depth in comparison to the relative fluctuations in the mass density, but the Ly α forest absorption cannot be associated with halos and the two assumptions above are not correct for this case.

4.4 Corrections for the two-point linear terms

Using the results above, we can now derive the correction to the bias factors measured from the total absorption field that includes the Ly α forest and the HCDs, to obtain the corrected bias factors of the Ly α forest:

$$\Delta b \equiv b_2 - b_\alpha = \frac{b_\alpha + b_H}{1 + C} - b_\alpha = -\frac{\bar{\tau}_{eH} b_h + C b_\alpha}{1 + C} \simeq -\bar{\tau}_{eH} b_h , \quad (4.20)$$

$$\Delta(b\beta) \equiv b_2 \beta_2 - b_\alpha \beta_\alpha = -\frac{\bar{\tau}_{eH} f(\Omega) + b_\alpha \beta_\alpha C}{1 + C} \simeq -\bar{\tau}_{eH} f(\Omega) , \quad (4.21)$$

$$\Delta\beta \equiv \beta_2 - \beta_\alpha = \frac{b_\alpha\beta_\alpha - \bar{\tau}_{eH}f(\Omega)}{b_2(1+C)} - \beta_\alpha = \frac{\bar{\tau}_{eH}[\beta_\alpha - f(\Omega)/b_h]}{b_\alpha/b_h - \bar{\tau}_{eH}}, \quad (4.22)$$

where the last expressions in equations (4.20) and (4.21) assume $C \ll 1$ (C is usually also substantially smaller than $\bar{\tau}_{eH}$ if this effective optical depth from HCDs is dominated by damped wings, which have little correlation with the Ly α forest). In Table 1 we show the value of C for the different mocks. Finally, the correction on the parameter that is best constrained from the 3D power spectrum is

$$\Delta(b + b\beta) = -\frac{\bar{\tau}_{eH}[b_h + f(\Omega)] + Cb_\alpha(1 + \beta_\alpha)}{1 + C} \simeq -\bar{\tau}_{eH}[b_h + f(\Omega)]. \quad (4.23)$$

The simple bias parameter corrections in equations 4.20, 4.21, 4.22 and 4.23 are plotted in Figure 7 as a function of $\bar{\tau}_{eH}$, for several values of b_h , and for the Ly α forest bias values used in our numerical mocks, $b_\alpha = -0.1375$ and $\beta_\alpha = 1.58$.

The effect of the HCDs can be mitigated if a large fraction of them can be individually detected in the absorption spectra, when the signal-to-noise is good enough. In a survey with similar characteristics as BOSS, one should be able to detect and mask most of the DLAs (with $N_{HI} > 10^{20.3} \text{ cm}^{-2}$), considerably reducing the value of $\bar{\tau}_{eH}$. The lower lines in Figure 2 show $1 - \bar{F}_H \simeq \bar{\tau}_{eH}$ when only systems of lower column densities are left. The effective optical depth from these systems is still about one third of that of all the HCDs.

However, masking and removing some of the HCDs before the flux correlation is measured may introduce potential problems. The HCDs are correlated with the Ly α forest, so if a portion of the spectrum around each HCD is simply eliminated from the data, we are introducing a bias that may be comparable or worse than the one caused by the HCDs themselves. Moreover, the HCDs that are detected may suffer from selection effects induced by the superposition of their damped wings with the Ly α forest. For example, HCDs living in large-scale regions with different values of η may have different probabilities of being detected because the Ly α forest absorption around them depends on η , and this would change the derived values of the b_η and β parameters. One should therefore be particularly careful if DLAs are masked and removed to precisely simulate the effect of this procedure in numerical mocks and see if the noise they introduce in the measurements can in fact be substantially reduced while any systematic effects that their removal may induce are properly corrected for.

4.5 Application to the measurement on mock spectra

Our simple analytical estimate for the systematic effect of HCDs on the bias parameters can now be compared to the numerical results obtained previously from mock spectra in the last section. Note that in our numerical mocks, $\beta_H = \beta_\alpha$ and $b'_{\eta H} = b_h\beta_\alpha/f(\Omega) \neq 1$, so equations (4.20), (4.21), (4.22) and (4.23) cannot be used, or must be modified to include the correct $b_{\eta H}$. Instead, we can use directly equations (4.16) and (4.17). The parameters for our fiducial mocks are $b_h = 1.21$, $\beta_h = \beta_\alpha = 1.58$, $C = 0.0034$, $b_\alpha = -0.1375$ and $\bar{\tau}_{eH} = 0.017$, which yield

$$\Delta b = -0.02, \quad \Delta\beta = 0 \quad \Delta b(1 + \beta) = -0.052. \quad (4.24)$$

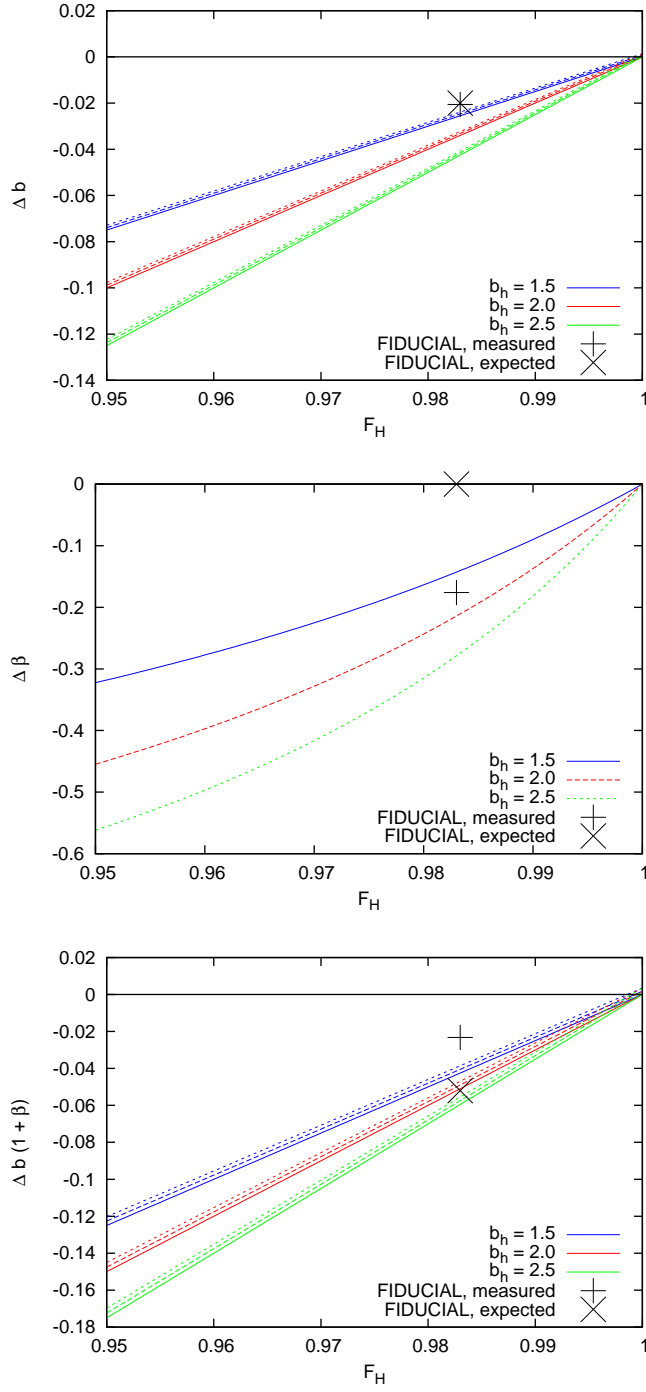


Figure 7. Correction to bias parameters as a function of halo bias b_h . Solid, dashed and dotted lines correspond to different values of C (0,0.01,0.005). Crosses show the analytical prediction for the FIDUCIAL mocks, and the actual measurement from the mocks.

These corrections from the simple two-point, linear model are shown as crosses in Figure 7. Clearly, other effects must be important in changing the best fit bias factors in the mocks,

in which the value of β is substantially decreased by the HCDs.

There are two reasons for the discrepancies between the analytically predicted corrections to the bias parameters and the actual corrections found in the mocks. One is the presence of the 3-point term $\xi_{3\alpha}$, the dominant one among the terms in ξ_{34} (eq. 4.9) that are not taken into account. However, Figure 6 shows that this term contributes only $\sim 2\%$ to the total correlation function, and is ~ 5 times smaller than the two-point terms, so it is surprising that its impact on the fitted values of the bias parameters of the numerically obtained correlation function may be so large.

A clue to what is going on is found in Table 1, where the model NO WINGS (in which the damped wings of the HCDs are eliminated) shows practically no correction on β_F . This model has a value of $\bar{\tau}_{eH} = 0.0068$, so we would expect the correction on β_F to be about three times smaller than for the FIDUCIAL model under no other changes, but the change on β_F is actually 30 times smaller. This strongly suggests that the reason for the discrepancy is to be found in the effect of the damped wings.

4.6 The non-linear effect of the damped wings

The damped wings imply that the linear theory approximation is not actually valid even on very large scales. The damped absorption falls as the inverse square of the line-of-sight separation, a dependence that is comparable to the rate of decrease of the correlation function. Therefore, the actual correlation function that is observed is not the linear theory expression derived from the power spectra in equation (4.15), but is the convolution along the line of sight of this linear correlation function with the Voigt profile of the average column density in HCDs that is correlated with the Ly α forest absorption.

Quantitatively, the linear form of the cross-correlation $\xi_{\alpha H}(\mathbf{x}_\perp, v)$, where the parallel component of the separation v is assumed to be expressed as a velocity, assumes that the absorption of a HCD is localized into an interval much narrower than the separation v . The damped wings imply that this is not actually true, and that the absorption has the Voigt profile $V(N, v' - v)$ at a velocity v' , for an absorber located at v with a column density N . Then, if the probability distribution of N is proportional to $f(N)$, and neglecting any effects of blending of the HCD profiles among themselves, the cross-correlation of the Ly α and HCD absorption is modified to a function $\xi_{\alpha H}^V$ equal to

$$\xi_{\alpha H}^V(\mathbf{x}_\perp, v) = \frac{\int dv'/c \int_{N_{LL}}^\infty dN f(N) V(N, v' - v) \xi_{\alpha H}(\mathbf{x}_\perp, v')}{\int_{N_{LL}}^\infty dN f(N) W(N)/\lambda_\alpha}, \quad (4.25)$$

where $W(N)$ is the rest-frame equivalent width of an absorber of column density N , and $N_{LL} = 10^{17.2} \text{ cm}^{-2}$. The linear form for the cross-correlation $\xi_{\alpha H}$ in redshift space is readily obtained from the equations in [16], replacing β for $(\beta_\alpha + \beta_H)/2$ and β^2 for $\beta_\alpha \beta_H$, and the convolution in the above equation can be computed and used in the model to fit the observed correlation function, by approximating $\xi_F \simeq \xi_2$ and replacing $\xi_{\alpha H}$ by $\xi_{\alpha H}^V$ in equation (4.8). Although we have not carried out this procedure for our mocks in this paper, our analysis in this section and the results in Figure 6 indicate that if this improved model is directly fitted to the data, the effects of HCDs ought to be corrected for to a high accuracy.

A similar approach was used in the Appendix B of [17].

5 Effect of Metal Lines

Apart from HCDs, the other contaminating absorption that is found in the spectral range where the Ly α forest is observed is from absorption lines of ionized heavy elements, or metals. When the transmission fraction is measured at a certain pixel, part of the absorption may be caused by any of the numerous intergalactic metal lines that are present in the ultraviolet spectrum. For metal lines with wavelengths close to that of the hydrogen Ly α line, their absorption can overlap with nearby, and therefore correlated, Ly α absorption. This introduces new components to the total transmission correlation, which will appear as peaks in the three-dimensional correlation centered on the line of sight at a velocity separation corresponding to the rest-frame wavelength separation of the metal and Ly α line. In the same way, pairs of metal lines overlapping the Ly α forest will also introduce peaks in the correlation function at the wavelength separation of each pair of metal lines.

Although we shall not treat the impact of metals in detail in this paper, we introduce here the general formalism for metal line corrections to the overall transmission correlation that is analogous to the one used for HCDs, which we believe will be useful for treating their effect. Let the transmitted fraction field of each one of the metal lines, i , that may appear in the spectral region of the Ly α forest, be $F_i = \bar{F}_i(1 + \delta_i)$. In this section, the Ly α transmission is not separated into a Ly α forest and HCD part, for simplicity. The total transmission fraction field that is measured is

$$F = F_\alpha \prod_i F_i ; \quad (5.1)$$

$$\bar{F}(1 + \delta_F) = \bar{F}_\alpha \prod_i \bar{F}_i (1 + \delta_\alpha) (1 + \delta_i) . \quad (5.2)$$

We now define the following two-point cross-correlations:

$$\xi_{\alpha i}(\mathbf{x}) = \langle \delta_\alpha(\mathbf{r})\delta_i(\mathbf{r} + \mathbf{x}) \rangle + \langle \delta_\alpha(\mathbf{r})\delta_i(\mathbf{r} - \mathbf{x}) \rangle ; \quad (5.3)$$

$$\xi_{ij}(\mathbf{x}) = \langle \delta_i(\mathbf{r})\delta_j(\mathbf{r} + \mathbf{x}) \rangle + \langle \delta_i(\mathbf{r})\delta_j(\mathbf{r} - \mathbf{x}) \rangle . \quad (5.4)$$

As usual, brackets denote ensemble averages over all pixel pairs separated by \mathbf{x} . Let λ_i be the central wavelength of each metal line i , and let the vector \mathbf{x}_i be directed along the line of sight with its radial component equal to $x_i = cH^{-1}(\lambda_i - \lambda_\alpha)/\lambda_\alpha$. The symmetrized cross-correlation $\xi_{\alpha i}$ then has two peaks, at $\mathbf{x} = \pm\mathbf{x}_i$, corresponding to the possibilities of having the Ly α line near \mathbf{r} and the metal line near $\mathbf{r} + \mathbf{x}$, or the Ly α line near $\mathbf{r} - \mathbf{x}$ and the metal line near \mathbf{r} [and two peaks at $\pm(\mathbf{x}_i - \mathbf{x}_j)$ for ξ_{ij}]. In the linear regime, these cross-correlations are simply the Fourier transforms of analogous power spectra to those in equations (4.13) and (4.14), which can be modeled in terms of bias factors and redshift distortion factors for each metal line, b_i and β_i , defined as in equations (4.10) and (4.11), and related to the bias factors of their host halos and their mean effective optical depth in full analogy to equations (4.19) for the HCDs. Therefore, the two-point correlations $\xi_{\alpha i}$ and ξ_{ij} are fully specified by these factors as long as the linear regime approximation is valid.

We define also:

$$C_m = \bar{F}/(\bar{F}_\alpha \prod_i \bar{F}_i) = 1 + \sum_i \xi_{\alpha i}(0) + \sum_{ij} \xi_{ij}(0) + \dots , \quad (5.5)$$

where we have omitted the three-point and higher-point functions. Note that C_m is nearly equal to unity, because the displacements x_i are usually large (the largest contributions to C_m should arise from lines with a wavelength close to that of Ly α , e.g., from SiIII), so the correlations at zero separation are very small.

The observed absorption perturbation field δ_F is then

$$C_m \delta_F = (1 + \delta_\alpha) \prod_i (1 + \delta_i) - C_m . \quad (5.6)$$

Evaluating the correlation of δ_F , and keeping only the most important terms, which are the two-point functions and the three-point term that contains only one metal contribution, we have

$$\begin{aligned} C_m^2 \xi_F(\mathbf{x}) = & - (C_m - 1)^2 + \xi_\alpha(\mathbf{x}) + \sum_i \xi_{\alpha i}(\mathbf{x}) + \sum_i \xi_{ii}(\mathbf{x}) + \sum_{i < j} \xi_{ij}(\mathbf{x}) + \\ & + \sum_i \langle \delta_\alpha(\mathbf{r}) \delta_\alpha(\mathbf{r} \pm \mathbf{x}) \delta_i(\mathbf{r}) \rangle \end{aligned} \quad (5.7)$$

where the symbol \pm implies here that there are two terms in the sum, one with the $+$ sign and one with the $-$ sign.

Ignoring the last three-point term, which is probably very small (and may be computed numerically in simple models where metal lines are added in mocks with a similar prescription as the one we have used for HCDs, and can probably also be modeled as a product of the two correlations $\xi_{\alpha i}$ and ξ_α), this shows that the effect of every metal line is fully specified by the parameters b_i and β_i , which can be related to the physical bias parameters of the host halos through the mean effective optical depth of every line, $\bar{\tau}_{ei}$. All these parameters should be directly measurable from the data, by extracting the shape of the peaks of the overall transmission correlation near the peak positions \mathbf{x}_i . Obviously these measurements will not be possible for weak metal lines as the peaks they create become buried into the noise, but it should still be possible to obtain combined measurements of the parameters for a set of metal lines that are assumed to be hosted by the same halos (and therefore have the same values of b'_i and β_i as in equations 4.19). This leads to a proposed outline for a program to be carried out to investigate all of the metal lines that can be statistically detected: to measure their parameters $\bar{\tau}_{ei}$, b_i and β_i and to use the formalism presented here to correct for their impact on the overall transmission correlation function.

6 Conclusions

The measurement of the bias and redshift distortion parameters of the Ly α forest correlation function may reveal essential characteristics of the physical evolution of the intergalactic medium. However, their values are affected by the presence of the absorption profiles from high column density systems (HCDs) and metal lines in the observed spectra. It is therefore necessary to study how these systems affect the correlation function to try to correct the measured parameters for their effect.

We have presented a numerical method to simulate the effect of HCDs (HCD) on the measured correlation function of the Ly α absorption, in which the Voigt profiles of absorbers

are inserted in mock spectra of the Ly α forest in positions that are correlated with the Ly α optical depth. We have evaluated the increase of the noise in the correlation measurement and the systematic change that is introduced in the recovered bias parameters owing to the correlation of HCDs with the Ly α forest. Both effects are very substantial: the HCDs contribution to the noise is close to that of the Ly α forest itself, and the bias parameters are altered by $\sim 10\%$ in the models we have used. Even though most of the increase in the noise is caused by damped Ly α systems that can individually be identified in the spectra, and therefore removed to reduce the noise, this should be considered as a dangerous operation to do because the identified systems that can be detected may have different bias factors, and therefore cause different systematic effects, than the set of all HCDs. If the removal of detected HCDs is attempted (either by masking regions of the spectrum where HCDs are present or fitting their profiles as part of the continuum), one should examine the difference in the results of the Ly α correlation measurements when no HCDs are removed, and test the selection of HCDs and their effects through simulations using mock spectra in which HCDs are inserted with the observed correlation with the Ly α forest.

An analytical formalism has also been developed to more generally predict the changes induced by HCDs on the inferred linear bias parameters. We find that the most important terms biasing the correlation function can be computed from the two-point cross-correlations of the Ly α and HCD absorption perturbation fields. Assuming the validity of linear theory and that HCDs are associated with their host halos in a way that is independent of the large-scale environment, we have inferred a set of simple equations relating the corrections on the bias factors to the effective optical depth and the host halos bias factor of the HCDs. The density bias factor is increased in absolute value by the product of the mean effective optical depth and the bias factor of the host halos of the HCDs (eq. 4.20), and the redshift distortion parameter is altered also in proportion to $\bar{\tau}_{eH}$ and the difference $\beta_\alpha - \beta_H$ (eq. 4.22)

Even though the results that can be derived analytically go in the direction of the correction to the fitted density bias factor that we find numerically for the specific model of the mocks we have analyzed, they do not quantitatively agree. We have identified two reasons for this discrepancy: one is the neglect of the three-point and four-point terms in the analytical approach, in particular the term $\xi_{3\alpha}$ in equations (4.5) and (4.6). The other one is the deviation from the linear theory form of the cross-correlation of the Ly α forest and HCD absorption due to the extended nature of the damped absorption profiles. The latter effect, in particular, should mostly explain the change in the total flux redshift distortion parameter, β_F , in our mocks (see Table 1), despite the fact that by construction, the HCDs are inserted with a distribution obeying $\beta_H = \beta_\alpha$. The damped wing profiles are acting analogously to “fingers of God” in galaxy redshift surveys to distort the contours of the correlation function and reduce the fitted value of β_F .

The results of this paper lead us to believe that it is possible to accurately correct for the contamination introduced by HCDs in the total transmission correlation function ξ_F , to infer the true underlying Ly α correlation function ξ_α , and therefore to constrain our models for the evolution of the intergalactic medium. In principle, by simply convolving the linear theory form of the cross-correlation function $\xi_{\alpha H}$ with a Voigt profile in the radial direction that results from the mean column density in HCDs associated with a Ly α forest transmission perturbation δ_α , one should have a much more accurate model to be fitted to the observations. The effect of the next largest term, $\xi_{3\alpha}$, can be numerically taken into account

once the parameters for the HCD model (mainly b_H , β_H and $\bar{\tau}_{eH}$) have been calibrated through the observational determination of the Ly α forest - HCD cross-correlation.

Although we have not attempted an evaluation of the impact of metal lines on the correlation function in this paper, we have proposed a basic formalism to understand and correct for their effect that is similar to the one for HCDs. For the metal lines that contaminate the spectral region of the Ly α forest, the metal-Ly α cross-correlations can also be measured from the data and its effect included when the observations of the overall flux correlation ξ_F are fitted. We are therefore optimistic on the prospects for obtaining accurate measurements of the Ly α correlation as a probe to the large-scale primordial perturbations and the physical evolution of the intergalactic medium from the BOSS and other future spectroscopic surveys of the Ly α forest.

Acknowledgements

We would like to thank Patrick McDonald, Matt McQuinn, Uros Seljak, Patrick Petitjean, and Anze Slosar for many illuminating discussions. We also thank CITA for their hospitality and the use of their computer resources by A. Font-Ribera to accomplish part of this work. This work was supported in part by Spanish grants AYA2009-09745 and PR2011-0431.

References

- [1] D. J. Eisenstein, D. H. Weinberg, E. Agol, H. Aihara, C. Allende Prieto, S. F. Anderson, J. A. Arns, É. Aubourg, S. Bailey, E. Balbinot, and et al., *SDSS-III: Massive Spectroscopic Surveys of the Distant Universe, the Milky Way, and Extra-Solar Planetary Systems*, *AJ* **142** (Sept., 2011) 72–+, [[arXiv:1101.1529](#)].
- [2] P. McDonald, *Toward a Measurement of the Cosmological Geometry at $z \sim 2$: Predicting Ly α Forest Correlation in Three Dimensions and the Potential of Future Data Sets*, *Astrophys. J.* **585** (Mar., 2003) 34–51, [[astro-ph/](#)].
- [3] N. Kaiser, *Clustering in real space and in redshift space*, *Mon. Not. Roy. Astron. Soc.* **227** (July, 1987) 1–21.
- [4] A. Slosar, A. Font-Ribera, M. M. Pieri, J. Rich, J.-M. Le Goff, É. Aubourg, J. Brinkmann, N. Busca, B. Carithers, R. Charlassier, M. Cortês, R. Croft, K. S. Dawson, D. Eisenstein, J.-C. Hamilton, S. Ho, K.-G. Lee, R. Lupton, P. McDonald, B. Medolin, D. Muna, J. Miralda-Escudé, A. D. Myers, R. C. Nichol, N. Palanque-Delabrouille, I. Pâris, P. Petitjean, Y. Piškur, E. Rollinde, N. P. Ross, D. J. Schlegel, D. P. Schneider, E. Sheldon, B. A. Weaver, D. H. Weinberg, C. Yèche, and D. G. York, *The Lyman- α forest in three dimensions: measurements of large scale flux correlations from BOSS 1st-year data*, *JCAP* **9** (Sept., 2011) 1–+, [[arXiv:1104.5244](#)].
- [5] A. Slosar, S. Ho, M. White, and T. Louis, *The acoustic peak in the Lyman alpha forest*, *JCAP* **10** (Oct., 2009) 19–+, [[arXiv:0906.2414](#)].
- [6] P. McDonald, U. Seljak, R. Cen, P. Bode, and J. P. Ostriker, *Physical effects on the Ly α forest flux power spectrum: damping wings, ionizing radiation fluctuations and galactic winds*, *Mon. Not. Roy. Astron. Soc.* **360** (July, 2005) 1471–1482.
- [7] M. Viel, M. G. Haehnelt, R. F. Carswell, and T.-S. Kim, *The effect of (strong) discrete absorption systems on the Lyman α forest flux power spectrum*, *Mon. Not. Roy. Astron. Soc.* **349** (Apr., 2004) L33–L37.

- [8] A. Font-Ribera, P. McDonald, and J. Miralda-Escudé, *Generating mock data sets for large-scale Lyman- α forest correlation measurements*, JCAP **1** (Jan., 2012) 1, [[arXiv:1108.5606](#)].
- [9] J. X. Prochaska, S. Herbert-Fort, and A. M. Wolfe, *The SDSS Damped Ly α Survey: Data Release 3*, Astrophys. J. **635** (Dec., 2005) 123–142, [[astro-ph/](#)].
- [10] P. Noterdaeme, P. Petitjean, C. Ledoux, and R. Srianand, *Evolution of the cosmological mass density of neutral gas from Sloan Digital Sky Survey II - Data Release 7*, A&A **505** (Oct., 2009) 1087–1098, [[arXiv:0908.1574](#)].
- [11] Z. Zheng and J. Miralda-Escudé, *Self-shielding Effects on the Column Density Distribution of Damped Ly α Systems*, Astrophys. J. Let. **568** (Apr., 2002) L71–L74.
- [12] J. X. Prochaska and A. M. Wolfe, *On the Kinematics of the Damped Lyman- α Protogalaxies*, Astrophys. J. **487** (Sept., 1997) 73, [[astro-ph/](#)].
- [13] L. Jiang, X. Fan, R. J. Cool, D. J. Eisenstein, I. Zehavi, G. T. Richards, R. Scranton, D. Johnston, M. A. Strauss, D. P. Schneider, and J. Brinkmann, *A Spectroscopic Survey of Faint Quasars in the SDSS Deep Stripe. I. Preliminary Results from the Co-added Catalog*, AJ **131** (June, 2006) 2788–2800, [[astro-ph/](#)].
- [14] P. McDonald, J. Miralda-Escudé, M. Rauch, W. L. W. Sargent, T. A. Barlow, R. Cen, and J. P. Ostriker, *The Observed Probability Distribution Function, Power Spectrum, and Correlation Function of the Transmitted Flux in the Ly α Forest*, Astrophys. J. **543** (Nov., 2000) 1–23.
- [15] C. M. Hirata, *Tidal alignments as a contaminant of redshift space distortions*, Mon. Not. Roy. Astron. Soc. **399** (Oct., 2009) 1074–1087, [[arXiv:0903.4929](#)].
- [16] A. J. S. Hamilton, *Measuring Omega and the real correlation function from the redshift correlation function*, Astrophys. J. Let. **385** (Jan., 1992) L5–L8.
- [17] M. McQuinn and M. White, *On estimating Ly α forest correlations between multiple sightlines*, Mon. Not. Roy. Astron. Soc. **415** (Aug., 2011) 2257–2269, [[arXiv:1102.1752](#)].

A Appendix: Clustering of the HCD systems

In this Appendix we show that the method described in Section 2 distributes the HCDs following a correlation function $\xi_h(\mathbf{r})$ in redshift space that is, on large scales, proportional to the flux correlation function $\xi_F(\mathbf{r})$. This implies that the redshift space distortion parameters of the two correlations are equal, $\beta_h = \beta_\alpha$. Furthermore, the ratio of these two correlations yields the relation between the bias factors of the distribution of HCDs and of the transmitted flux fraction field, b_h and b_F ,

$$\frac{\xi_h(\mathbf{r})}{\xi_F(\mathbf{r})} = \left(\frac{b_h}{b_F} \right)^2. \quad (\text{A.1})$$

To simplify our notation in this Appendix, we use F , \bar{F} and ξ_F to refer to the Ly α forest variables that in the main text are referred to as F_α , \bar{F}_α and ξ_α .

The method to generate the mock Ly α absorption field, described in detail in [8] and summarized in Section 2, generates first a random Gaussian field δ_g with a correlation function $\xi_g(\mathbf{r})$, such that the final flux field $F(\delta_g)$ has the desired correlation $\xi_F(\mathbf{r})$, as well as the desired probability distribution function $p_F(F)$. We first prove that this auxiliary Gaussian field has the same correlation function as the flux field, with a different bias parameter b_g . Then we show that the peaks of the Gaussian field also have the same correlation function, with a relative bias set by the peak threshold.

A.1 Biases of the Gaussian field

The relation between the correlation of any function $F(\delta_g)$ and ξ_g can be computed as follows:

$$\begin{aligned}
\bar{F}^2[1 + \xi_F(\mathbf{r}_{12})] &= \langle F(\mathbf{x}_1) F(\mathbf{x}_2) \rangle = \int_0^1 dF_1 \int_0^1 dF_2 p_F(F_1, F_2) F_1 F_2 \\
&= \int_{-\infty}^{\infty} d\delta_{g1} \int_{-\infty}^{\infty} d\delta_{g2} p_g(\delta_{g1}, \delta_{g2}) F(\delta_{g1}) F(\delta_{g2}) \\
&= \int_{-\infty}^{\infty} d\delta_{g1} \int_{-\infty}^{\infty} d\delta_{g2} \frac{\exp\left[-\frac{\delta_{g1}^2 + \delta_{g2}^2 - 2\delta_{g1}\delta_{g2}\xi_g(r_{12})}{2[(1 - \xi_g^2(\mathbf{r}_{12}))]} \right]}{2\pi\sqrt{1 - \xi_g^2(\mathbf{r}_{12})}} F(\delta_{g1}) F(\delta_{g2}) ,
\end{aligned} \tag{A.2}$$

In the method to generate the Ly α mocks, this expression is inverted to find ξ_g as a function of the desired ξ_F . In this Appendix we use it to show that, on large scales, the two correlation functions are proportional to each other.

The Gaussian variables $\delta_{g1} = \delta_g(\mathbf{x}_1)$ and $\delta_{g2} = \delta_g(\mathbf{x}_2)$ are normalized to unit dispersion and their correlation is $\xi_g(\mathbf{r}_{12})$. We define the new normal variables y_1, y_2 as linear combinations that are independent:

$$\delta_{g1} = y_1 ; \quad \delta_{g2} = \xi_g y_1 + \sqrt{1 - \xi_g^2} y_2 . \tag{A.3}$$

In the linear regime, we can assume $\xi_g \ll 1$ and use a first-order expansion of the function $F(\delta_{g2})$,

$$F(\delta_{g2}) \approx F(y_2) + \frac{dF}{d\delta_g} y_1 \xi_g = F(y_2) \left(1 - \frac{d\tau}{d\delta_{g2}} y_1 \xi_g \right) , \tag{A.4}$$

where $\tau = -\ln(F)$.

The flux correlation in equation (A.2) now becomes,

$$\bar{F}^2[1 + \xi_F(\mathbf{r}_{12})] \approx \int_{-\infty}^{\infty} dy_1 p_g(y_1) F(y_1) \int_{-\infty}^{\infty} dy_2 p_g(y_2) F(y_2) \left(1 - \frac{d\tau}{dy_2} y_1 \xi_g \right) , \tag{A.5}$$

where $p_g(y)$ is the one-dimensional, normal Gaussian distribution. Requiring now that $\xi_F(\mathbf{r}_{12}) = (b_F/b_g)^2 \xi_g(\mathbf{r}_{12})$, we find that the ratio of bias parameters is fully determined by the transformation $F(\delta_g)$:

$$\left(\frac{b_F}{b_g} \right)^2 = \frac{1}{\bar{F}^2} \int_{-\infty}^{\infty} dy_1 p_g(y_1) F(y_1) y_1 \int_{-\infty}^{\infty} dy_2 p_g(y_2) F(y_2) \frac{d\tau}{dy_2} . \tag{A.6}$$

The mocks used in this paper are computed using a lognormal transformation for the optical depth τ ,

$$F(\delta_g) = \exp[-\tau(\delta_g)] = \exp\left[-ae^{\gamma\delta_g}\right] , \tag{A.7}$$

with $a = 0.077$ and $\gamma = 2.16$. Using this transformation, the ratio of the bias factors is

$$\left(\frac{b_F}{b_g} \right)^2 = 0.0925 . \tag{A.8}$$

A.2 Biases of the peaks

In section 2 we describe a method to distribute HCD systems in regions of the Ly α spectra where the optical depth is above a threshold τ_c or, equivalently, above a threshold δ_{gc} in the Gaussian variable used to generate the optical depth. We refer to these regions as *peaks*. The threshold sets the fraction ν of pixels that are candidates to host a HCD:

$$\nu = \int_{\delta_{gc}}^{\infty} d\delta_g p_g(\delta_g) . \quad (\text{A.9})$$

The correlation function of these peaks, ξ_h , is related to the probability of having a peak both at $\delta_{g1} = \delta_g(\mathbf{x}_1)$ and at $\delta_{g2} = \delta_g(\mathbf{x}_2)$:

$$\begin{aligned} p(\delta_{g1} > \delta_{gc}, \delta_{g2} > \delta_{gc}) &= \nu^2 [1 + \xi_h(\mathbf{r}_{12})] \\ &= \int_{\delta_{gc}}^{\infty} d\delta_{g1} \int_{\delta_{gc}}^{\infty} d\delta_{g2} p_g(\delta_{g1}, \delta_{g2}) \\ &= \int_{\delta_{gc}}^{\infty} d\delta_{g1} \int_{\delta_{gc}}^{\infty} d\delta_{g2} \frac{\exp\left[-\frac{\delta_{g1}^2 + \delta_{g2}^2 - 2\delta_{g1}\delta_{g2}\xi_g(\mathbf{r}_{12})}{2[1 - \xi_g^2(\mathbf{r}_{12})]}\right]}{2\pi\sqrt{1 - \xi_g^2(\mathbf{r}_{12})}} . \end{aligned} \quad (\text{A.10})$$

We now express δ_{g1} and δ_{g2} as a function of the independent normal variables y_1 and y_2 defined in equation A.3. Defining $\delta'_{gc}(y_1, \xi_g) = (\delta_{gc} - y_1\xi_g)/(1 - \xi_g^2)^{1/2}$, we obtain

$$\begin{aligned} \nu^2 (1 + \xi_h) &= \int_{\delta_{gc}}^{\infty} dy_1 p_g(y_1) \int_{\delta'_{gc}(y_1, \xi_g)}^{\infty} dy_2 p_g(y_2) \\ &= \int_{\delta_{gc}}^{\infty} dy_1 p_g(y_1) \times \left[\int_{\delta'_{gc}(y_1, \xi_g)}^{\delta_{gc}} dy_2 p_g(y_2) + \int_{\delta_{gc}}^{\infty} dy_2 p_g(y_2) \right] \\ &\approx \int_{\delta_{gc}}^{\infty} dy_1 p_g(y_1) \{ [\delta_{gc} - (\delta_{gc} - y_1\xi_g)] p_g(\delta_{gc}) + \nu \} \\ &= \nu^2 \left[1 + \left(\frac{b_h}{b_g}\right)^2 \xi_g \right] , \end{aligned} \quad (\text{A.11})$$

where b_g and b_h are the bias parameters of the Gaussian field and the peaks, respectively. The bias ratio is then a function of ν only:

$$\left(\frac{b_h}{b_g}\right)^2 = \frac{p_g(\delta_{gc})}{\nu^2} \int_{\delta_{gc}}^{\infty} dy_1 p_g(y_1) y_1 . \quad (\text{A.12})$$

For the values used in the models in this paper, we find $b_h/b_g = 2.66$ for $\nu = 0.01$, and $b_h/b_g = 3.18$ for $\nu = 0.002$. Using equation (A.8) and the value of the Ly α forest bias in our mocks, $b_F = -0.1375$, we find the bias of the HCD systems to be $b_h = 1.21$ for $\nu = 0.01$, and $b_h = 1.43$ for $\nu = 0.002$.

Finally, because the correlation of the peaks has been shown to be proportional to the correlation of the Gaussian field, their redshift distortion parameter must be the same.